

Structure of complement fragment C3b–factor H and implications for host protection by complement regulators

Jin Wu¹, You-Qiang Wu², Daniel Ricklin², Bert J C Janssen¹, John D Lambris^{2,3} & Piet Gros^{1,3}

Factor H (FH) is an abundant regulator of complement activation and protects host cells from self-attack by complement. Here we provide insight into the regulatory activity of FH by solving the crystal structure of the first four domains of FH in complex with its target, complement fragment C3b. FH interacted with multiple domains of C3b, covering a large, extended surface area. The structure indicated that FH destabilizes the C3 convertase by competition and electrostatic repulsion and that FH enables proteolytic degradation of C3b by providing a binding platform for protease factor I while stabilizing the overall domain arrangement of C3b. Our results offer general models for complement regulation and provide structural explanations for disease-related mutations in the genes encoding both FH and C3b.

The efficacy of the complement-mediated immune response relies on a delicate balance between activation and regulation. Although continuous generation of the strong opsonin complement fragment C3b by the alternative pathway allows rapid reaction to foreign or abnormal cells, its indiscriminate deposition may potentially cause host tissue damage. Host cells are therefore protected by proteins of the regulator of complement activation (RCA) family, which either impair the generation of new C3b by accelerating the decay of the C3 convertases or act as cofactor for factor I (FI) in degrading existing C3b^{1,2}. In addition to cell surface-bound RCA proteins such as decay-accelerating factor (DAF (A000571); also called CD55), membrane cofactor protein (MCP (A000568); also called CD46) and complement receptor 1 (CR1; also called CD35), the soluble and highly abundant regulator factor H (FH) offers an additional layer of protection, as it controls the steady-state alternative pathway activation in circulation. Furthermore, FH may be recruited to host membranes by recognizing and binding self components, such as glycosaminoglycans, and thereby may prevent the opsonization of host tissue with low surface expression of RCA^{1,3}.

The importance of FH in maintaining a well-balanced immune response is reflected by the increasing number of diseases found to have strong association with mutations and polymorphisms in the gene encoding FH, as found in age-related macular degeneration (AMD), atypical hemolytic uremic syndrome (aHUS) and membranoproliferative glomerulonephritis type II (MPGN-II)^{4,5}. Several pathogenic microorganisms evade attack of the complement cascade by expressing structural homologs of FH or by recruiting host FH to their surfaces via FH-binding proteins^{6,7}. Owing to their vital function

in immune modulation, therapeutic targeting of FH as well as other RCA proteins is considered important for the treatment of diseases associated with abnormal or loss of complement control^{8,9}.

FH is formed by a linear string of complement control protein (CCP) domains that consist of about 60 residues and are common to all RCA proteins¹. The first four domains (CCP1–CCP4) of FH are necessary and sufficient for regulation of complement in the fluid phase, whereas host cell specificity is determined by domains CCP5–CCP20 of FH^{1,10,11}. Despite a wealth of functional and structural data on the CCP domains of various complement regulators, understanding of the two molecular mechanisms that protect host cells, referred to as ‘decay-acceleration activity’ and ‘cofactor activity’, still remains limited.

Here we provide insight into the mechanisms of host protection against complement activation by presenting the crystal structure of the four functional domains of FH (CCP1–CCP4) in complex with C3b. By combining our structural model with biochemical and biophysical data as well as with findings from previous mutational studies, we are able to delineate individual processes and correlate disease-related mutations with functional consequences. Furthermore, our findings allow us to extrapolate these results to other members of the RCA family and to develop a more general model for complement regulation.

RESULTS

Crystal structure of C3b–in complex with FH domains 1–4

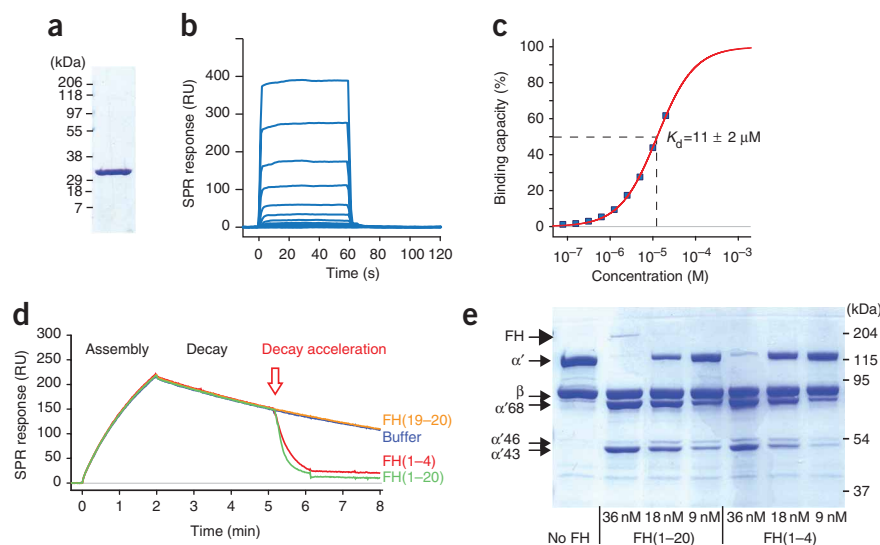
For this study, we expressed the amino (N)-terminal four CCP domains (amino acid residues 1–246) of FH (called ‘FH(1–4)’ here), which are known to mediate both of the regulatory activities of

¹Crystal and Structural Chemistry, Bijvoet Center for Biomolecular Research, Department of Chemistry, Faculty of Science, Utrecht University, Utrecht, The Netherlands.

²Department of Pathology & Laboratory Medicine, University of Pennsylvania, Philadelphia, Pennsylvania, USA. ³These authors contributed equally to this work. Correspondence should be addressed to P.G. (p.gros@uu.nl) or J.D.L. (lambris@upenn.edu).

Received 11 March; accepted 14 May; published online 7 June 2009; doi:10.1038/ni.1755

Figure 1 Characterization of recombinant FH(1–4). **(a)** Purity of FH(1–4), as assessed by SDS-PAGE (4–15% gradient gel; reducing conditions; Coomassie blue staining). Data are representative of more than five experiments with various conditions. **(b,c)** Direct binding of soluble FH(1–4) to surface-bound C3b. Injection of the FH fragment (0.08–20 μM) leads to the formation of a short-lived 1:1 complex with C3b **(b)** with a binding affinity (dissociation constant (K_d)) of $11 \pm 2 \mu\text{M}$ **(c)**. SPR, surface plasmon resonance. Data are representative of five experiments with different surface densities of C3b (3,000–7,000 resonance units (RU)). **(d)** Decay-acceleration activity of FH(1–4) and full-length FH (FH(1–20)) when injected onto surface-based C3 convertase (C3bBb); (additional details and control injections, **Supplementary Fig. 9** online). Data are representative of three independent experiments. **(e)** Cofactor activity of FH(1–4) and FH, assessed by incubation of C3b with FI and increasing amounts of either FH(1–4) or FH(1–20), leading to the generation of iC3b, as indicated by degradation of the α' chain to three fragments of 43, 46 and 68 kDa ($\alpha'43$, $\alpha'46$ and $\alpha'68$, respectively; left margin). Data are representative of more than five individual experiments.



FH¹⁰ (**Fig. 1a**). This recombinant FH(1–4) bound C3b with an affinity of 11 μM (measured as the dissociation constant; **Fig. 1b,c**) and was functionally active *in vitro* in terms of both decay acceleration and cofactor activity (**Fig. 1d,e**). We crystallized the complex of C3b-FH(1–4) and determined the structure to a resolution of 2.7 \AA (**Fig. 2** and **Table 1**). The structure showed a large and discontinuous interface between FH(1–4) and C3b that stretched over a distance of 100 \AA and buried a surface area of about 4,500 \AA^2 (**Fig. 2a**). Despite the putative flexibility between individual CCP domains of FH, FH(1–4) bound to C3b showed only small differences in domain orientations compared with the nuclear magnetic resonance (NMR) structures of CCP1–CCP2 and CCP2–CCP3 (ref. 12). The tilt angle between CCP1 and CCP2 was altered by about 10°, which led to closer proximity of CCP1 to C3b (**Fig. 2b** and **Supplementary Table 1** online). There was a kink between CCP3 and CCP4 that was responsible for the overall L-shaped appearance of FH(1–4), which is consistent with small-angle X-ray-scattering data of CCP1–CCP5 of FH¹³. The structure of C3b showed its typical arrangement of 12 domains formed by the β -chain (amino acid residues 1–645) and the α' chain (amino acid residues 727–1641)^{14,15}, obtained after proteolytic activation of the native C3 (**Fig. 2**). The core of the structure was formed by eight macroglobulin (MG) domains and a linker domain. Inserted between MG7 and MG8 were a CUB domain ('complement C1r-C1s, UEGF, BMP1') and a thioester-containing domain (TED), which allows covalent attachment to target surfaces. The carboxyl (C) terminus was extended by a C345C domain, which is common to complement components C3, C4 and C5. We found two differences in domain orientations in C3b-FH(1–4) versus unbound C3b: the C-terminal C345C domain was repositioned, which we attributed to differences in crystal packing, and the CUB domain and TED were rotated by about 12° (refs. 14,15; **Fig. 2b** and **Supplementary Figs. 1** and **2** online). The change in CUB and TED was probably due to interactions with FH(1–4); however, variations in CUB-TED positioning have been reported for other structures of C3b^{14,15} (**Fig. 2b** and **Supplementary Fig. 1**).

The C3b-FH(1–4) interface consisted of four contact regions spanning the length of FH(1–4) (**Fig. 3** and **Supplementary Table 2** online). The bottom half of CCP1 and the CCP1–CCP2 linker attached through hydrophobic interactions and salt bridges to the acidic α' N-terminal (α' NT) region (amino acid residues 727–746)

and the MG7 domain in C3b. Antibody binding to MG7–MG8 inhibited the interaction of C3b with both FH(1–4) and full-length FH¹⁶ (**Supplementary Fig. 3** online), which confirms that the α' NT and MG7 region is a primary binding site for FH^{17,18}. The second main binding site involved a patch of conserved hydrophobic residues surrounded by hydrophilic residues on CCP2 that interacted with MG6 of C3b (**Fig. 2a** and **Supplementary Figs. 4** and **5** online). At the third site, CCP3 contacted residues of both the α' -chain and β -chain of C3b and bridged MG2 and CUB, which contains the three scissile bonds that are cleaved by FI. Notably, the hypervariable loop of CCP3 of FH (amino acid residues 139–145) that was disordered in the published NMR structure¹² was ordered in the C3b-FH(1–4) complex

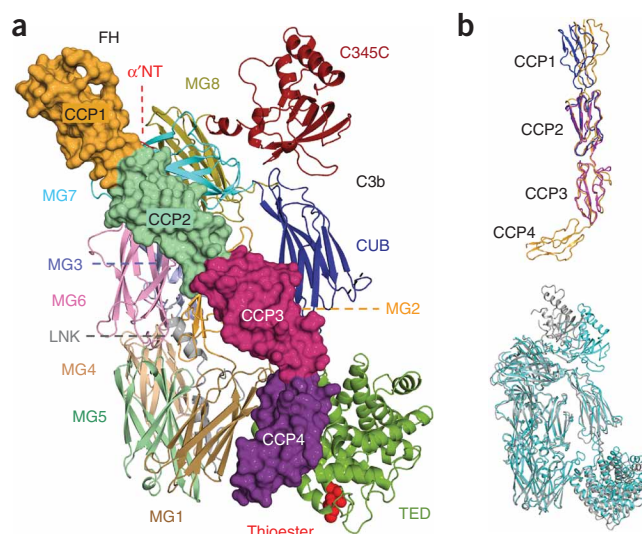


Figure 2 Structure of C3b in complex with FH(1–4). **(a)** Overall structure of the C3b-FH(1–4) complex. C3b is presented as a 'ribbon' and FH is presented as surface representations; red spheres indicate thioesters. **(b)** Top, FH(1–4) in complex (orange) with NMR structures of CCP1–CCP2 (blue) and CCP2–CCP3 (magenta)¹²; bottom, C3b in complex with FH(1–4) (cyan) and free C3b (gray)¹⁴. Diagrams were generated with the PyMOL molecular visualization system.

Table 1 Data collection and refinement statistics

Data collection	
Space group	$P2_12_12$
Cell dimensions	
<i>a</i> , <i>b</i> , <i>c</i> (Å)	223.5, 84.9, 128.8
Resolution (Å)	67–2.7 (2.85–2.7)
R_{merge} (%)	11.3% (60.8%)
<i>I</i> / σ <i>i</i>	8.3 (1.9)
Completeness (%)	99.7 (100)
Redundancy	3.7 (3.8)
Refinement statistics	
Resolution (Å)	64.5–2.7
Reflections	67,893
$R_{\text{work}}/R_{\text{free}}$ (%)	21.7/25.2
Atoms	14,442
Protein	14,081
Ligand/ion	189
Water	172
B-factors (Å ²)	
Protein	68.2
Ligand/ion	106.7
Water	48.2
r.m.s.d.	
Bond lengths (Å)	0.002
Bond angles (°)	0.446

Values in parentheses are for the shell of highest resolution.

and interacted with the CUB domain of C3b. At the fourth and final site, CCP4 formed another bridge between MG1 and TED, which we confirmed by blocking experiments with a TED-specific antibody (**Supplementary Fig. 3**). The arrangement of the α NT, MG7, CUB and TED domains are known to change considerably during the conversion of C3 to C3b^{14,15,19,20}, which explains the specificity of FH for C3b rather than C3. In summary, the complex showed an extensive interface that involved many domains of C3b and all domains of FH(1–4), a result that is supported by the binding studies reported here (**Fig. 1b,c** and **Supplementary Fig. 4**) and in published reports^{16–18}.

Structural basis of decay-acceleration activity

The ability of FH(1–4) to dissociate the protease fragment (Bb) from the alternative pathway C3 convertase complex (C3b–Bb; **Fig. 1d**) suggested competition for the same binding region on C3b. We therefore compared the structure of C3b–FH(1–4) with that of the convertase stabilized by the staphylococcal inhibitor SCIN²¹ (**Fig. 4a**) by superimposing the β -chains of the C3b molecules of both complexes. The superposition showed a large steric clash between CCP1–CCP2 of FH(1–4) and the Bb fragment of the convertase. The N-linked glycan at the asparagine residue at position 260 (Asn260) in Bb contributed to the observed clash (**Supplementary Fig. 6** online). In agreement with that finding, deletion of this glycan by the substitution N260D renders the convertase less sensitive to decay acceleration²². In addition to steric hindrance, the complementary surfaces of FH and Bb were both negatively charged (**Fig. 4b**), which indicates that electrostatic repulsion contributed to the destabilization of the C3bBb complex. These results indicate a functional role for CCP1–CCP2 in displacing Bb and a supportive role for CCP3–CCP4 in binding to C3b.

To propose a general model of decay acceleration, we compared our data with the structure and mutagenesis data of DAF^{23,24}. Overlay of the functional CCP2–CCP3 domains of DAF onto CCP1–CCP2 of FH showed that DAF had similar residues at the C3b contact sites (**Supplementary Fig. 5**). Moreover, residues critical for DAF activity, which are located in the CCP2–CCP3 linker and on the CCP3 surface, faced Bb in the C3bBb complex²⁴ (**Fig. 4c**). Similar to the binding of FH, the proposed binding mode of DAF resulted in steric overlap with Bb. However, the critical residues on DAF facing Bb in the C3bBb complex were mainly hydrophobic and not negatively charged, as in the case of FH (**Fig. 4b,c** and **Supplementary Fig. 5**). The hydrophobic patch on DAF faced the β F- α 7 loop of the von Willebrand factor A (VWA) domain in Bb (**Fig. 4a,c**). This section of the VWA domain was hidden in the proenzyme FB, which possibly explains why DAF binds Bb but hardly binds full-length FB²⁵. Interaction of DAF with this loop may induce a low affinity state of the metal ion-dependent adhesion site in Bb and thereby disrupt the C3bBb complex, similar to the allostery in integrin I domains²⁶. However, the structural observations do not readily explain the effects of substitutions at Lys298 and Tyr338 in FB on the decay-acceleration activity of DAF, CR1 and FH^{22,27}. It is possible that these substitutions in the VWA domain, distal from the RCA-interaction side, may affect the allosteric mechanism.

Implications for cofactor activity

FH supported two of three possible cleavages in the CUB domain of C3b by FI (between Arg1281 and Ser1282 and between Arg1298 and Ser1299) that yield the inactive iC3b species²⁸ (**Fig. 1e**). The crystal structure showed that CCP2–CCP3 of FH bound to C3b adjacent to the CUB domain (**Figs. 2a** and **5a**), with the hypervariable loop of CCP3 directly contacting the CUB domain¹⁰ (**Fig. 5**). Cleavage site Arg1281–Ser1282 was well exposed, whereas Arg1298–Ser1299 was occluded in the complex (**Fig. 5b**), which confirms the idea that Arg1281–Ser1282 is cleaved first and suggests that cleavage of Arg1298–Ser1299 requires conformational changes. The strong influence of ionicity on the binding of FI indicates that polar interactions are important for this interaction²⁹. CCP1–CCP3 of FH indeed showed several conserved and charged patches on its surface (**Fig. 5a** and **Supplementary Fig. 7** online), which may be involved in the binding of FI. For the FH homolog vaccinia virus complement control protein (VCP), CCP2 has been shown to have a dominant function in complement inhibition. Substitution of four residues in

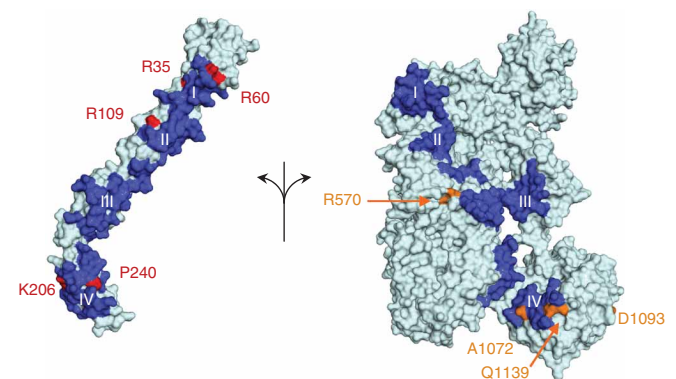


Figure 3 Mapping of FH and C3 mutants on the complex structure. Molecules are presented in surface representation with FH(1–4) on the left and C3b on the right. The four contact regions (I–IV) between FH(1–4) and C3b are in blue, with substitutions linked to AMD, MPGN-II and aHUS in red (for FH mutants) or orange (for C3b mutants).

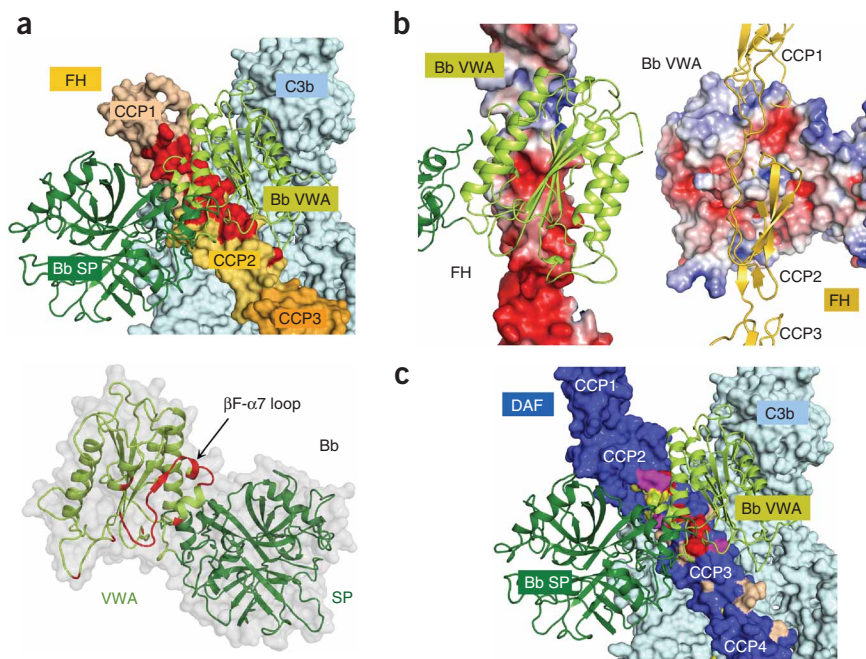


Figure 4 Structural basis of decay-acceleration activity. (a) Overlay of the C3b-FH and C3bBb complexes²¹ (top) with C3b (light cyan) and CCP1-CCP3 of FH (beige, yellow-orange and orange, respectively) in surface representation and Bb in ribbon representation (light green, VWA domain; dark green, serine protease (SP) domain); the red surface area indicates the region where FH and Bb overlap (atomic distances of less than 2 Å). Below, overlap region (red) in Bb (Bb is rotated by 180° relative to the diagram above). (b) Electrostatic surface potential of FH and ribbon representation of Bb (left) and vice versa (right) in the regions facing each other. Potential contours are presented on a scale from $-5 k_B T e_c^{-1}$ (red) to $+5 k_B T e_c^{-1}$ (blue), where k_B is the Boltzmann constant, T is absolute temperature and e_c is elementary charge. (c) Superposition of CCP2-CCP4 of DAF²³ onto CCP1-CCP3 of FH, presented as in (a). Colors of DAF substitutions indicate the degree of functional interference, from minor (beige), medium (yellow) and severe (magenta) to complete abortion (red) of decay acceleration by DAF²⁴.

CCP2 markedly enhances cofactor activity, although it only moderately increases the affinity of VCP for C3b³⁰. The equivalent residues in FH (Gln101, Ile106, Asp112 and Asp119) were fully exposed and were adjacent to conserved patches (Fig. 5a), which suggests involvement of these four residues in the binding of FI. Furthermore, studies of cobra venom factor have indicated that the C345C domain of C3b may contribute to this interaction³¹. These data suggest that FI binds the C3b-FH complex at the area formed by CCP1-CCP3 of FH and by C345C and CUB of C3b (Supplementary Fig. 7). In addition to providing a platform for FI, FH may have a second function in cofactor activity; we hypothesize that the bridge formed by CCP4 between TED and the core of C3b may maintain the position of TED while the connecting CUB domain undergoes further cleavage. This suggested function is supported by disease-related mutations in the sequence encoding CCP4 of FH^{32,33} and in the sequence encoding TED of C3b³⁴, which indicates functional importance for interactions of RCA proteins with TED.

Mapping of disease-related mutations

The complex structure provided a structural basis for understanding the effects of six disease-related mutations that can be found in the sequence encoding domains CCP1-CCP4 of FH. In a first step, we examined two substitutions (R60G and P204L) and one deletion (K206Δ) located directly at the C3b-FH(1-4) interface (Fig. 3). In case of the aHUS-related mutant R60G³⁵, a salt bridge between the guanidium group of Arg60 in CCP1 of FH and the acidic Asp732 of α' NT in C3b was lost by the substitution (Supplementary Fig. 8a online). In CCP4 of FH, the backbone amide of Lys206 formed a hydrogen bond with the carboxylate of Glu1138 in TED, whereas the lysine side chain formed an intramolecular

salt bridge with the carboxylate of Glu213 (Supplementary Fig. 8b). The MPGN-II-associated deletion of this residue probably alters the local structure in CCP4, which would explain the diminished binding to C3b and loss of regulatory functions of FH³². In the aHUS-related mutant P240L³³, the *cis*-peptide conformation of Pro240 is probably essential for the binding of CCP4 in a pocket formed by both MG1 and TED of C3b (Supplementary Fig. 8c), and its substitution may directly affect the C3b-FH interaction. The remaining three substitutions (V44I, R35H and R109L) were not located at the C3b-FH interface (Supplementary Fig. 8d,e). The V44I mutant is not only associated with AMD and MPGN-II (refs. 36,37) but also has been shown to have a strong association with polypodial choroidal vasculopathy³⁸. Val44 is part of the hydrophobic core of the

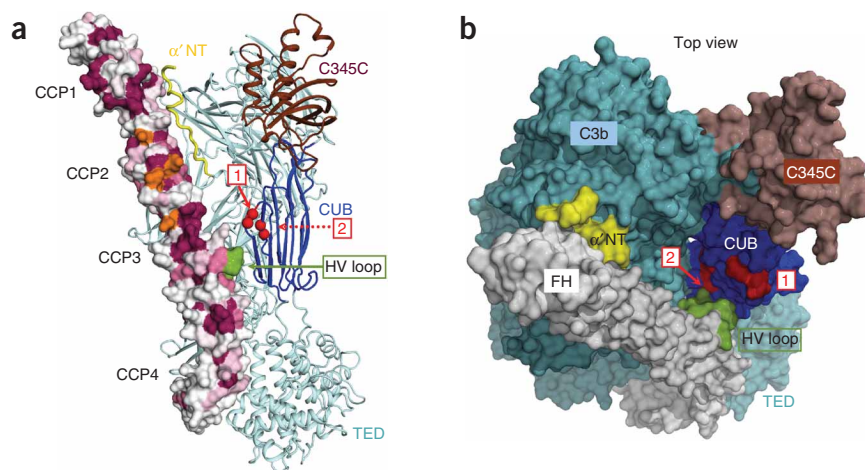


Figure 5 Structural implications of cofactor activity. (a) Sites of FI binding and cleavage. FH is presented in surface representation; colors indicate residue conservation with mutational data from ref. 30. Residues with the conservation scores of less than 5 are white; substitutions in VCP that enhance FI binding are orange; the hypervariable loop (HV loop) of CCP3 is green. C3b is cyan, with the CUB (blue), α' NT (yellow) and C345C (dark red) domains highlighted and the first and second scissile bonds in the CUB domain indicated by red spheres (conservation scale and corresponding colors, Supplementary Fig. 4). (b) Surface representation of the complex from the top view. Colors of the domains and FI cleavage sites are as in (a); FH domains are gray.

CCP1 domain and may therefore affect domain stability. Indeed, NMR studies have demonstrated an effect on the thermal stability of V44I, whereas only subtle structural differences could be detected between wild-type and mutant proteins¹². Arg35 of the aHUS-related substitution R35H³³ was solvent exposed and was located on the bottom part of CCP1 opposite the C3b-interaction surface (**Supplementary Fig. 8d**). Although few structural rearrangements have been reported for the R35H mutant¹², its localization on the putative FI-interaction face of FH may affect binding to FI. The substitution R109L has been found in two patients with MPGN-II (ref. 39). As the hydrophobic portion of the arginine side chain was buried in the hydrophobic core of the CCP2 domain packing against the conserved Trp116 residue (**Supplementary Fig. 8e**), this substitution possibly affects the folding or stability of the CCP2 domain.

Many aHUS-linked mutations have also been described for the gene encoding C3 (ref. 34); they have large effects on C3b-MCP binding and smaller effects on C3b-FH binding. Substitutions R570Q or R570W, A1072V and Q1139K were all located at the C3b-FH interface (**Fig. 3**) and decreased the binding of FH by 10–50% (ref. 34). For R570Q and R570W, the replacement of Arg570 may lead to a loss of electrostatic interactions (at a distance of 4 Å) with Glu98 of FH (**Supplementary Fig. 8f**). In the A1072V mutant, the bulkier side chain of valine may sterically hinder interactions with Tyr225 of FH (**Supplementary Fig. 8g**) and diminish C3b-FH binding. Substitution Q1139K introduces a positive charge that possibly leads to a salt bridge between Lys1139 and the preceding Asp1138 (**Supplementary Fig. 8h**) and probably modifies interactions with FH. Other substitutions in TED, such as D1093N (**Fig. 3**), may not be connected with FH(1–4) but instead may be connected with the secondary C3b binding site at CCP19–CCP20 (ref. 11).

DISCUSSION

Tight regulation of the complement response on host cells and in the circulation is critical for providing selectivity against foreign cells and preventing complement-mediated tissue damage. Given their essential function in immune response and the increasing number of diseases with known or suspected involvement of complement regulators, detailed knowledge about the underlying molecular processes is very much desired. Our data are important in this context, as they have yielded a structure of C3b in complex with a complement regulator. Our results not only provide insight into the function of the most abundant regulator, FH, but also allow us to develop more general models of complement regulation. In agreement with published observations¹⁰, the N-terminal 4 of 20 CCP domains of FH were functionally sufficient and showed both decay-acceleration and cofactor activity. FH(1–4) bound C3b in an extended configuration, which resulted in a long contact interface that covered the entire flank of C3b. The interface involved all four N-terminal CCP domains of FH and many domains of C3b, including α 'NT, MG1, MG2, MG6, MG7, CUB and TED. Despite this large interface, the binding affinity of the two molecules was rather low, with a dissociation constant of 11 μ M. This result is in agreement with a published study comparing the binding affinities of several FH fragments to C3b and is in a range similar to that of FH(19–20) but much weaker than that of full-length FH¹¹.

The structure of the C3b-FH(1–4) complex provides a molecular basis for understanding the two regulatory mechanisms, decay-acceleration activity and cofactor activity, by which proteins of the RCA family protect host cells. On the basis of structural comparisons of C3b-FH(1–4) and C3bBb²¹, we conclude that decay acceleration is mediated mainly by the first two N-terminal CCP domains of FH,

which bind the α 'NT and MG2 and MG6–MG7 domains of C3b. These domains probably dislocate the Bb protease fragment by electrostatic repulsion and steric hindrance from the convertase. The conserved location of functional residues in the homologous domains CCP2–CCP3 of DAF suggest that similar displacement effects are also involved in case of this regulator²⁴. Nevertheless, DAF and FH may differ in their precise mechanisms of dislocating Bb from C3b, as direct interaction with Bb has been reported for DAF but not for FH²⁵. We therefore hypothesize that DAF interacts with the β F- α 7 loop of the VWA domain in Bb and hence induces a low-affinity conformation of the metal ion-dependent adhesion site that mediates binding of Bb to the C terminus of C3b. More structural data, such as C3b-DAF and DAF-Bb complexes, are needed to understand the differences in the precise mechanisms of DAF and FH.

Our data further suggest that the cofactor activity of FH in the conversion of C3b to the inactive iC3b species is based on two essential mechanisms. First, FH provides a contact interface for the initial binding of the protease FI to the C3b-regulator complex and brings it into close proximity to the CUB domain of C3b. The four N-terminal CCP domains of FH bind along the CUB domain of C3b. This structural arrangement suggests that FI may bind CCP1–CCP3 of FH and C345C of C3b, a proposal that is supported by VCP mutagenesis data³⁰ and studies of cobra venom factor chimeras³¹. Although FI is reported to bind directly yet weakly to C3b in the absence of FH, the binding affinity substantially increases after the addition of FH²⁹. The newly formed extended binding site between FH and C3b probably considerably improves the FI binding affinity and, as a consequence, the cleavage rate. Secondly, FH enables the sequential cleavage of C3b through stabilization of the TED-CUB arrangement relative to the core of the C3b molecule. We have shown that domain CCP4 bridges the TED and MG1 domains of C3b and we argue that these interactions keep TED in place during cleavage by FI. In contrast to FH, MCP does not bind to the α 'NT region of C3b, which explains its lack of decay-acceleration activity^{17,18}. The cofactor activity of MCP, in contrast, may be mediated in a way similar to that of FH. Binding experiments analyzing disease-related mutations have indicated that MCP also binds C3b through MG6 and TED³⁴. Several of the C3 mutants that showed much less C3b-MCP binding have substitutions such as R570Q, R570W, A1072V and Q1139K that are all at the C3b-FH interface³⁴. However, the exact binding arrangement is probably different for the two regulators, as the C3b-binding site in domain CCP4 of MCP, as derived from mutagenesis studies⁴⁰, does not coincide fully with the corresponding site in CCP4 of FH.

FH has experienced increasing interest in biomedical sciences during the past decade as it has become evident that mutations and polymorphisms of the gene encoding this regulator are strongly associated with diseases such as aHUS, AMD and MPGN-II (refs. 33,34). In AMD, mutation of the gene encoding FH is even considered the most consistent genetic risk factor⁴¹. Although some effects may be attributed to altered binding of glycosaminoglycan or changes in the secondary C3b binding site on CCP19–CCP20, other substitutions are located in CCP1–CCP4 and were therefore mapped on the C3b-FH(1–4) structure. Our analysis indicates that disruption of specific contacts (such as salt bridges) or the induction of local conformational changes may substantially alter the C3b-FH interface. The specific yet rather weak interaction between C3b and FH(1–4) may be essential for fast and selective complement regulation but also makes FH prone to functional interference by even small modifications in its sequence. The substitutions described, therefore, probably weaken the affinity, which may lead to a loss of regulatory activity and, finally, to apparent disease states.

In conclusion, our structural data provide an important framework for understanding the two key molecular mechanisms of host protection by RCA proteins: decay-acceleration activity and cofactor activity. We have also offered a basis for explaining the functional consequences of individual substitutions related to dysfunctional complement regulation and associated diseases. Thus, our study may pave the way for the development of therapeutics directed at modulating complement activation.

METHODS

Methods and any associated references are available in the online version of the paper at <http://www.nature.com/natureimmunology/>.

Accession codes. UCSD-Nature Signaling Gateway (<http://www.signaling-gateway.org/>): A000571 and A000568; Protein Data Bank: Complement C3b in complex with factor H domains 1–4, 2WII.

Note: Supplementary information is available on the Nature Immunology website.

ACKNOWLEDGMENTS

We thank the European Synchrotron Radiation Facility for synchrotron radiation facilities; beamline scientists of the European Synchrotron Radiation Facility and the European Molecular Biology Laboratory for assistance; M. Pangburn (University of Texas at Tyler) for the CFH clone; P. Barlow (University of Edinburgh) for FH(19–20) protein; and M.A. Hadders for critical reading of the manuscript and comments. Supported by the Council for Chemical Sciences of the Netherlands Organization for Scientific Research (P.G.) and the US National Institutes of Health (J.D.L.).

AUTHOR CONTRIBUTIONS

J.W. purified C3 and C3b; Y.-Q.W. expressed and purified FH(1–4) and did cofactor assays; D.R. did decay acceleration, antibody competition and direct binding studies; J.W. crystallized the complex, collected data and determined, refined and analyzed the structure; B.J.C.J. helped with all stages of structure determination and analysis; J.D.L. and P.G. conceived and supervised the project; and J.W., D.R. and P.G. wrote the manuscript.

Published online at <http://www.nature.com/natureimmunology/>

Reprints and permissions information is available online at <http://npg.nature.com/reprintsandpermissions/>

- Schmidt, C.Q., Herbert, A.P., Hocking, H.G., Uhrin, D. & Barlow, P.N. Translational mini-review series on complement factor H: Structural and functional correlations for factor H. *Clin. Exp. Immunol.* **151**, 14–24 (2008).
- Liszewski, M.K., Farries, T.C., Lublin, D.M., Rooney, I.A. & Atkinson, J.P. Control of the complement system. *Adv. Immunol.* **61**, 201–283 (1996).
- Prosser, B.E. *et al.* Structural basis for complement factor H linked age-related macular degeneration. *J. Exp. Med.* **204**, 2277–2283 (2007).
- Meri, S. Loss of self-control in the complement system and innate autoreactivity. *Ann. NY Acad. Sci.* **1109**, 93–105 (2007).
- de Cordoba, S.R. & de Jorge, E.G. Translational mini-review series on complement factor H: genetics and disease associations of human complement factor H. *Clin. Exp. Immunol.* **151**, 1–13 (2008).
- Lambris, J.D., Ricklin, D. & Geisbrecht, B.V. Complement evasion by human pathogens. *Nat. Rev. Microbiol.* **6**, 132–142 (2008).
- Schneider, M.C. *et al.* *Neisseria meningitidis* recruits factor H using protein mimicry of host carbohydrates. *Nature* **458**, 890–893 (2009).
- Ricklin, D. & Lambris, J.D. Complement-targeted therapeutics. *Nat. Biotechnol.* **25**, 1265–1275 (2007).
- Noris, M. & Remuzzi, G. Translational mini-review series on complement factor H: therapies of renal diseases associated with complement factor H abnormalities: atypical haemolytic uraemic syndrome and membranoproliferative glomerulonephritis. *Clin. Exp. Immunol.* **151**, 199–209 (2008).
- Gordon, D.L., Kaufman, R.M., Blackmore, T.K., Kwong, J. & Lublin, D.M. Identification of complement regulatory domains in human factor H. *J. Immunol.* **155**, 348–356 (1995).
- Schmidt, C.Q. *et al.* A new map of glycosaminoglycan and C3b binding sites on factor H. *J. Immunol.* **181**, 2610–2619 (2008).
- Hocking, H.G. *et al.* Structure of the N-terminal region of complement factor H and conformational implications of disease-linked sequence variations. *J. Biol. Chem.* **283**, 9475–9487 (2008).
- Okemefuna, A.I. *et al.* The regulatory SCR-1/5 and cell surface-binding SCR-16/20 fragments of factor H reveal partially folded-back solution structures and different self-associative properties. *J. Mol. Biol.* **375**, 80–101 (2008).
- Janssen, B.J., Christodoulidou, A., McCarthy, A., Lambris, J.D. & Gros, P. Structure of C3b reveals conformational changes that underlie complement activity. *Nature* **444**, 213–216 (2006).
- Wiesmann, C. *et al.* Structure of C3b in complex with CR1g gives insights into regulation of complement activation. *Nature* **444**, 217–220 (2006).
- Becherer, J.D., Alsenz, J., Esparza, I., Hack, C.E. & Lambris, J.D. Segment spanning residues 727–768 of the complement C3 sequence contains a neoantigenic site and accommodates the binding of CR1, factor H, and factor B. *Biochemistry* **31**, 1787–1794 (1992).
- Lambris, J.D. *et al.* Dissection of CR1, factor H, membrane cofactor protein, and factor B binding and functional sites in the third complement component. *J. Immunol.* **156**, 4821–4832 (1996).
- Oran, A.E. & Isenman, D.E. Identification of residues within the 727–767 segment of human complement component C3 important for its interaction with factor H and with complement receptor 1 (CR1, CD35). *J. Biol. Chem.* **274**, 5120–5130 (1999).
- Janssen, B.J. *et al.* Structures of complement component C3 provide insights into the function and evolution of immunity. *Nature* **437**, 505–511 (2005).
- Gros, P., Milder, F.J. & Janssen, B.J. Complement driven by conformational changes. *Nat. Rev. Immunol.* **8**, 48–58 (2008).
- Rooijackers, S.H.M. *et al.* Structural and functional implications of the complement convertase stabilized by a staphylococcal inhibitor. *Nat. Immunol.* advance online publication, doi:10.1038/ni.1756 (7 June 2009).
- Hourcade, D.E., Mitchell, L., Kuttner-Kondo, L.A., Atkinson, J.P. & Medof, M.E. Decay-accelerating factor (DAF), complement receptor 1 (CR1), and factor H dissociate the complement AP C3 convertase (C3bBb) via sites on the type A domain of Bb. *J. Biol. Chem.* **277**, 1107–1112 (2002).
- Lukacik, P. *et al.* Complement regulation at the molecular level: the structure of decay-accelerating factor. *Proc. Natl. Acad. Sci. USA* **101**, 1279–1284 (2004).
- Kuttner-Kondo, L. *et al.* Structure-based mapping of DAF active site residues that accelerate the decay of C3 convertases. *J. Biol. Chem.* **282**, 18552–18562 (2007).
- Harris, C.L., Abbott, R.J., Smith, R.A., Morgan, B.P. & Lea, S.M. Molecular dissection of interactions between components of the alternative pathway of complement and decay accelerating factor (CD55). *J. Biol. Chem.* **280**, 2569–2578 (2005).
- Luo, B.H., Carman, C.V. & Springer, T.A. Structural basis of integrin regulation and signaling. *Annu. Rev. Immunol.* **25**, 619–647 (2007).
- Goicoechea de Jorge, E. *et al.* Gain-of-function mutations in complement factor B are associated with atypical hemolytic uremic syndrome. *Proc. Natl. Acad. Sci. USA* **104**, 240–245 (2007).
- Sahu, A., Isaacs, S.N., Soulika, A.M. & Lambris, J.D. Interaction of vaccinia virus complement control protein with human complement proteins: factor I-mediated degradation of C3b to iC3b1 inactivates the alternative complement pathway. *J. Immunol.* **160**, 5596–5604 (1998).
- DiScipio, R.G. Ultrastructures and interactions of complement factors H and I. *J. Immunol.* **149**, 2592–2599 (1992).
- Yadav, V.N., Pyaram, K., Mullick, J. & Sahu, A. Identification of hot spots in the variola virus complement inhibitor (SPICE) for human complement regulation. *J. Virol.* **82**, 3283–3294 (2008).
- Fritzing, D.C. *et al.* Functional characterization of human C3/cobra venom factor hybrid proteins for therapeutic complement depletion. *Dev. Comp. Immunol.* **33**, 105–116 (2009).
- Licht, C. *et al.* Deletion of Lys224 in regulatory domain 4 of factor H reveals a novel pathomechanism for dense deposit disease (MPGN II). *Kidney Int.* **70**, 42–50 (2006).
- Saunders, R.E., Goodship, T.H., Zipfel, P.F. & Perkins, S.J. An interactive web database of factor H-associated hemolytic uremic syndrome mutations: insights into the structural consequences of disease-associated mutations. *Hum. Mutat.* **27**, 21–30 (2006).
- Fremaux-Bacchi, V. *et al.* Mutations in complement C3 predispose to development of atypical hemolytic uremic syndrome. *Blood* **112**, 4948–4952 (2008).
- Caprioli, J. *et al.* Complement factor H mutations and gene polymorphisms in haemolytic uraemic syndrome: the C-257T, the A2089G and the G2881T polymorphisms are strongly associated with the disease. *Hum. Mol. Genet.* **12**, 3385–3395 (2003).
- Hageman, G.S. *et al.* A common haplotype in the complement regulatory gene factor H (HF1/CFH) predisposes individuals to age-related macular degeneration. *Proc. Natl. Acad. Sci. USA* **102**, 7227–7232 (2005).
- Abraera-Abeleda, M.A. *et al.* Variations in the complement regulatory genes factor H (CFH) and factor H related 5 (CFHR5) are associated with membranoproliferative glomerulonephritis type II (dense deposit disease). *J. Med. Genet.* **43**, 582–589 (2006).
- Kondo, N., Honda, S., Kuno, S. & Negi, A. Coding variant I62V in the complement factor H gene is strongly associated with polypoidal choroidal vasculopathy. *Ophthalmology* **116**, 304–310 (2009).
- Dragon-Durey, M.A. *et al.* Heterozygous and homozygous factor h deficiencies associated with hemolytic uremic syndrome or membranoproliferative glomerulonephritis: report and genetic analysis of 16 cases. *J. Am. Soc. Nephrol.* **15**, 787–795 (2004).
- Liszewski, M.K. *et al.* Dissecting sites important for complement regulatory activity in membrane cofactor protein (MCP; CD46). *J. Biol. Chem.* **275**, 37692–37701 (2000).
- Coleman, H.R., Chan, C.C., Ferris, F.L. III & Chew, E.Y. Age-related macular degeneration. *Lancet* **372**, 1835–1845 (2008).

ONLINE METHODS

Protein expression and purification. C3 was isolated from human plasma. After informed consent was provided by the donor, plasma was obtained at the University Medical Center Utrecht according to a study protocol approved by the medical ethics committee of the University Medical Center Utrecht. C3b was generated by limited trypsin treatment of C3 as described^{19,42} with some modifications (**Supplementary Methods** online). The DNA fragment encoding human FH domains CCP1–CCP4 (residues 1–246) was amplified by PCR from the full-length *CFH* clone and was ligated into the pSecTag2 B vector (Invitrogen). Recombinant FH(1–4), which contains a c-Myc tag and six-histidine tag at its C terminus, was expressed in human embryonic kidney HEK293T cells with plasmids with polyethenimine (linear, ~25 kDa; Poly-sciences) and was incubated in Hybridoma-SFM (Gibco-Invitrogen) containing 1% (vol/vol) FBS (HyClone). Medium was collected 4 d after transfection and was concentrated before protein purification. FH(1–4) was purified by metal-affinity chromatography (Ni-NTA Superflow; Qiagen) and was eluted with 200 mM imidazole in PBS, pH 8.0. All protein-containing fractions were pooled and were dialyzed against 10 mM phosphate buffer, pH 7.4, and were further purified by ion-exchange chromatography with a Resource Q column (GE Healthcare BioSciences) with a linear gradient of 0–300 mM NaCl over 30 column volumes. Purified FH(1–4) was dialyzed against 10 mM Tris, 50 mM NaCl, pH 7.4 and was concentrated to 1.7 mg/ml before crystallization. The purity of FH(1–4) was verified by SDS-PAGE.

Crystallization, data collection and structure determination. Purified C3b (30 mg/ml) and FH(1–4) (1.7 mg/ml) were mixed at a molar ratio of 1:1 to a final concentration 8.5 mg/ml (40 μ M) of the complex. C3b-FH(1–4) was crystallized in 7.0% (wt/vol) PEG 3,350 and 70 mM ammonium acetate, pH 7.1, by hanging-drop vapor diffusion at 18 °C. Crystals appeared after 2 d and grew within 5 d to a typical size of 200 \times 100 \times 60 μ m. Crystals were soaked for several minutes in reservoir solution supplemented with 20% (vol/vol) glycerol and then were ‘flash-cooled’ in liquid nitrogen. Crystals belong to space group $P2_12_12$ ($a = 223.5$ Å, $b = 84.9$ Å, $c = 128.8$ Å), and the best crystal diffracted to a resolution of 2.7 Å at European Synchrotron Radiation Facility beamline ID14-EH4. Diffraction data were integrated and scaled with the programs MOSFLM and Scala⁴³. The structure of C3b-FH(1–4) was determined by molecular replacement with the program PHASER⁴⁴. First, the β -chain (residues 1–642) of C3c (Protein Data Bank accession code 2A74)¹⁹ was placed, followed by the stepwise addition of the TED, CUB and α NT-MG7-MG8 domains from C3b (Protein Data Bank accession code 2I07)¹⁴. The initial models for the individual CCP domains of FH were generated by the program Chainsaw⁴⁵ with structures of CCP2 of human β_2 -glycoprotein I (Protein Data Bank accession code 1QUB; residues 63–121)⁴⁶ and CCP4 of DAF (Protein Data Bank accession code 1H03; residues 130–191)²³ as templates. The CCP2 and CCP3 domains of FH were found, but molecular-replacement searches of domains CCP1 and CCP4 initially failed. The C345C domain of C3b was then successfully placed with the C345C domain from the C3c structure (residues 1496–1641) as search model. The Chainsaw model for the fourth CCP domain of FH was placed manually with the Crystallographic Object-Oriented Toolkit⁴⁷, based on an $F_o - F_c$ (observed structure factor – calculated structure factor) difference map and subsequently refined as a rigid body in PHASER. After several rounds of refinement and model building with the Crystallographic Object-Oriented Toolkit, the bottom part of CCP1 (20 of

65 residues in total) could be built manually. The complete CCP1 derived from the NMR structure of CCP1–CCP2 of FH (Protein Data Bank accession code 2RLP; residues 2–64)¹² was then placed by superposition and rigid-body refinement in PHASER to obtain the complete model. The model was refined with the macromolecular refinement program REFMAC⁴⁸ and the PHENIX software suite⁴⁹. The final model, consisting of 1,536 residues of C3b and 244 residues of FH(1–4), had R_{work} and R_{free} values of 21.7% and 25.2%, respectively.

Binding-affinity assay. Surface plasmon resonance was used to determine the binding affinity of soluble FH(1–4) for C3b immobilized specifically by its thioester as described in the **Supplementary Methods**.

Complement decay-acceleration activity and cofactor activity. The decay-acceleration activity of the alternative pathway of complement activation was assessed by surface plasmon resonance. On-chip formation and decay of the C3 convertase were assessed by injection of an equimolar mixture of factor B and factor D (100 nM each) on immobilized C3b (**Supplementary Methods**) for 2 min at a flow rate of 10 μ l/min in HEPES-buffered saline–Mg²⁺ buffer (10 mM HEPES, 150 mM NaCl, 0.005% (vol/vol) Tween-20 and 1 mM MgCl₂, pH 7.4). After an undisturbed decay phase of 3 min, 200 nM FH(1–20), FH(1–4), FH(19–20) or a buffer control was injected for 1 min and the decrease in baseline after injection was evaluated. For removal of residual interactants, the surface was regenerated with 1 μ M FH(1–4) and 1 M NaCl. Values for binding signals of the FH fragments with C3b (in absence of the convertase) were subtracted from the data set for visualization of the pure decay acceleration. The cofactor activity of FH(1–4) was tested with a published protocol⁵⁰. Human C3b (4 μ g; 1.14 μ M) and human factor I (10 ng; 8 nM) were incubated for 1 h at 37 °C with various amounts (9, 18, 36 nM) of FH(1–20) or FH(1–4) in PBS buffer in a final volume of 20 μ l. Reactions were stopped by the addition of SDS-PAGE loading buffer and samples were analyzed by 10% SDS-PAGE.

Antibody competition assay. Individual contact sites of FH(1–4) on C3b were confirmed by surface plasmon resonance with monoclonal antibodies to C3b (C3-9 and 311) as described in the **Supplementary Methods**.

42. Lambris, J.D., Dobson, N.J. & Ross, G.D. Release of endogenous C3b inactivator from lymphocytes in response to triggering membrane receptors for beta 1H globulin. *J. Exp. Med.* **152**, 1625–1644 (1980).
43. Evans, P. Scaling and assessment of data quality. *Acta Crystallographica Section D* **62**, 72–82 (2006).
44. McCoy, A.J. *et al.* Phaser crystallographic software. *J. Appl. Crystallogr.* **40**, 658–674 (2007).
45. Stein, N. CHAINSAW: a program for mutating pdb files used as templates in molecular replacement. *J. Appl. Crystallogr.* **41**, 641–643 (2008).
46. Bouma, B. *et al.* Adhesion mechanism of human β_2 -glycoprotein I to phospholipids based on its crystal structure. *EMBO J.* **18**, 5166–5174 (1999).
47. Emsley, P. & Cowtan, K. Coot: model-building tools for molecular graphics. *Acta Crystallogr. D Biol. Crystallogr.* **60**, 2126–2132 (2004).
48. Winn, M.D., Murshudov, G.N. & Papiz, M.Z. Macromolecular TLS refinement in REFMAC at moderate resolutions. *Methods Enzymol.* **374**, 300–321 (2003).
49. Adams, P.D. *et al.* PHENIX: building new software for automated crystallographic structure determination. *Acta Crystallogr. D Biol. Crystallogr.* **58**, 1948–1954 (2002).
50. Alsenz, J., Lambris, J.D., Schulz, T.F. & Dierich, M.P. Localization of the complement-component-C3b-binding site and the cofactor activity for factor I in the 38kDa tryptic fragment of factor H. *Biochem. J.* **224**, 389–398 (1984).